Detecting early damages in the railway pantograph mechanism: a multiple excitation approach for the frequency domain

G. Santamato, D. Chiaradia, M. Solazzi & A. Frisoli

Published online: 01 Aug 2023.

Submit your article to this journal ⧉

Article views: 235

View related articles ⧉

View Crossmark data ⧉

IA**VSD**

Taylor & Francis
Taylor & Francis Group

Detecting early damages in the railway pantograph mechanism: a multiple excitation approach for the frequency domain

G. Santamato[a,b], D. Chiaradia[a,b], M. Solazzi[a,b] and A. Frisoli[a,b]

[a]Institute of Mechanical Intelligence, Scuola Superiore Sant'Anna, Pisa, Italy; [b]Department of Excellence in Robotics & AI, Scuola Superiore Sant'Anna, Pisa, Italy

ABSTRACT

In this work, we address the problem of damage diagnosis on the railway pantograph mechanism including nonlinear behaviour and sample-induced uncertainties. In particular, we discuss an experimental campaign in which investigation pursued the analysis of frequency response functions estimated by a dedicated inspection robot that we intentionally developed for vibration tests on pantographs. Special focus is pointed to the inherent nonlinear behaviour of the pantograph for which we estimated the damage index for different levels of the input excitation. The investigation is carried out on a population of pantographs of the same type and studying three kinds of damages. Results highlight the relevance of including several excitation levels and encourage investigation in a real operational scenario.

1. Introduction

The railway pantograph is a linkage mechanism mounted on the roof of electric trains and devoted to collecting energy through the sliding contact between the high-voltage line and the pan head. Despite being an established technology, the interaction between the pantograph and the line still represents a concern for the operation and safety of the railway due to possible electric arcs and entanglements [1–3]. Dedicated research identified in certain dynamics characteristics of the pantograph the faults root causes: (i) significant variations of the uplift force [4]; (ii) excessive stiffness of the pan head suspension [5–7]; (iii) insufficient damping [5,6,8]; (iv) loss of member connectivity in the linkage frame [2]. Consequently, the periodic and/or continuous assessment of the pantograph mechanism is crucial to achieving stable contact with the line and reducing the risk of accidents and interruptions of the railway service.

Extensive research tackled the problem through numerical [9,10] and experimental simulations. Three-axis test benches were developed to simulate the interaction between the pantograph and the catenary [11,12]. A comprehensive comparison of these works is found in the study of Bruni [13]. In particular, some of these tools, such as PCADA [14], PantoCat

---

CONTACT G. Santamato ✉ giancarlo.santamato@santannapisa.it

[15], and OSCAR [16], are presently validated according to the European standard EN 50318:2018 [17].

A considerable number of patents have also been proposed for measuring the uplift force and/or the damping of the pantograph actuation [18–25] which are the fundamental features of the pantograph operation. Still, at the depots, visual and manual inspection is the most common approach for pantograph assessment. Nevertheless, verification of the complete opening and closure of the pantograph and/or rough estimation of the uplift force only allows the detection of gross damages, like large deformation of the arms and of the actuation organs. Inspection routines usually do not pursue an investigation of the dynamics even though for most engineering structures vibration-based damage diagnosis has become an established standard.

In this regard, the pantograph – being a linkage mechanism – implies some of the relevant challenges for a vibration-based structural health monitoring [26,27]:

- the presence of multiple no lubricated pinned joints, Figure 1(b), introduces inherent nonlinear behaviour, meaning that the response of the pantograph is already nonlinear in the undamaged condition, as shown in [7,28];
- significant uncertainties: pantograph samples – even belonging to the same type – may present gross variability in the mounting layout, the used components, and the dry-friction level.

In [7], Xin proposed a laboratory test rig for executing different kinds of tests, including vibration tests for the estimation of the Frequency Response Function (FRF). Pantograph nonlinearity was demonstrated by estimating the FRF at multiple displacement amplitudes ranging from 0.3 mm to 5 mm. The actuator was arranged by an industrial hoist that was simply supported on the pantograph head. Consequently, contact was lost behind a certain level of excitation, impeding an accurate investigation. Besides, no statistical analysis was included. To the best of the authors' knowledge, emerges a lack of extensive investigation on vibration tests for the fault diagnosis of the pantograph, dealing with nonlinearity and statistical analysis.

This paper addresses the problem of damage detection and identification in the structure of the pantographs mechanism including nonlinearity and uncertainties. Damage diagnosis is pursued through a non-parametric statistical method based on the identified FRFs of the pantograph in the safe (undamaged) and damaged condition [29]. The inherent nonlinear behaviour of the pantograph is addressed by carrying out structural dynamic tests for multiple levels of excitation to ascertain whether nonlinearity can be exploited for augmenting the information about the health status of the pantograph. To this end, we adopted, as the test rig, a dedicated inspection robot device, Figure 1, that we specifically realised for excitation, signals acquisition, data processing, and allowing fine control of the input excitation level [30], which is a crucial feature when dealing with nonlinear systems.

Besides, the typical large variability that occurs between different pantographs was also included by identifying the FRFs on different pantograph samples belonging to the same family type. Four pantographs were tested with different operational lives and aging conditions: three pantographs in the undamaged state were used to set up a baseline of reference, and one pantograph was devoted to simulating three damage conditions, affecting the block of the pan head suspensions, the hydraulic damper, and the integrity of a bolted joint.
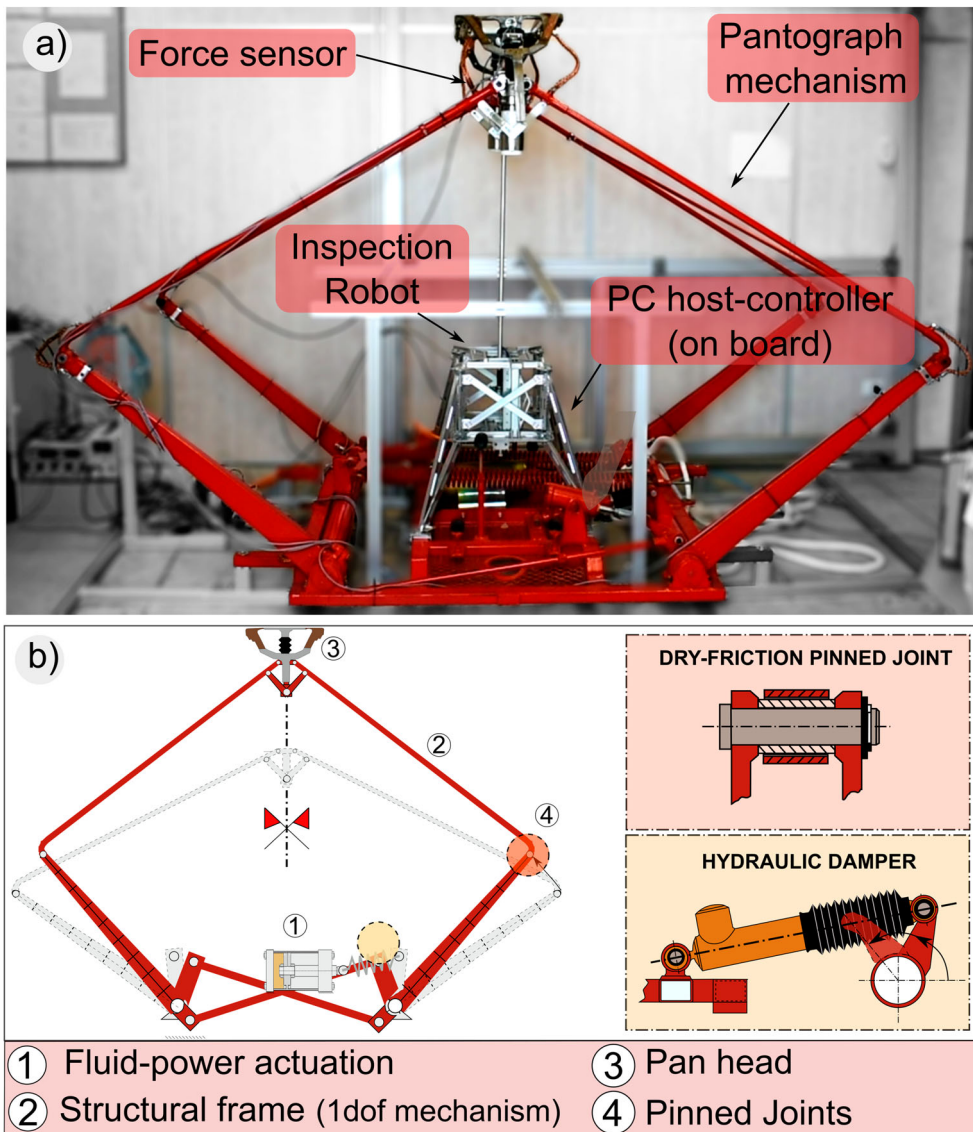
Figure 1. (a) A railway pantograph and the inspection robot that we designed for structural dynamic tests and fault diagnosis. Pictorial details of (b) the dry friction pinned joint as a main source of nonlinear frictional damping and hydraulic damper of the pantograph actuation.

The paper is structured as follows: in Section 2 we introduce the problem statement. The experimental equipment is discussed in Section 3, with a special focus on the robotic device and the strategy for fine control of the excitation force. For the sake of completeness, we describe a preliminary test designed to characterise the uplift force, the viscous damping, and the dry-fricion of the pantograph actuation. Section 4 is devoted to introducing the methodology for damage detection and indicative damage identification. We also describe the construction of a baseline as a reference of conformity.

The effects of the simulated damages on the FRF are presented in Section 5 where we analyse how the defined damage index is affected by the excitation level and whether false positives or false negatives have been found. Section 6 summarises the work and points out the future directions of research.

2. Problem statement and case study

The fundamentals of the present experimental case study are outlined in the following:

- Problem confronted:
  - ° the pantograph exhibits nonlinear behaviour both in safe (undamaged) and damaged conditions mainly due to dry-friction damping; as a consequence, multiple FRFs are collected for different levels of the input excitation through a dedicated inspection robot designed for accurate dynamic test on the pantographs;
  - ° an aggregated damage index is derived for each scenario (safe and damage) and for each level of the input excitation in order to assess whether the use of a low or a high vibration regime can be exploited to detect and identify the explored damage conditions.
- Experimental data variation:
  - ° the baseline for the undamaged state was constructed by acquiring the FRFs from a population of three undamaged pantographs, but characterised by distinct age, wear, and operational life;
  - ° the baseline experiments were performed with the same equipment, but in different facilities (overhaul and laboratory), and on different days;
  - ° additional response variation was included by restarting the experimental setup before the execution of tests in each considered scenario. Indeed, due to the combined effects of friction and play within the pinned joints, we observed a variation of the FRF estimated before and after the complete opening and closure maneuvers. This uncertainty was included to test the robustness of the damage diagnosis which is one of the objectives of our work.
- Three kinds of damage have been studied in this work:
  - ° block of the pan head suspensions (left, right, and combined: left + right);
  - ° exhausted hydraulic damper;
  - ° loss of member connectivity at a bolted connection.

3. Experimental setup

3.1. Equipment description and control of the excitation level

The adopted experimental setup is shown in Figure 2(a). The railway pantograph sample belongs to the type FS 52/92C with base encumbrance of $1800 \times 1350 \, \text{mm}^2$, a maximum head extension of 2200 mm, and a mass of the mechanism equal to 35 kg.

The inspection robot has a base encumbrance of $400 \times 400 \, \text{mm}^2$, a height of 600 mm, and a weight equal to 19.3 kg. The robot is endowed with a stinger actuator that drives the pantograph into forced vibrations. As indicated in Figure 2(a), the input is the dynamic force Q applied by the robot along the vertical direction at the driven-point,
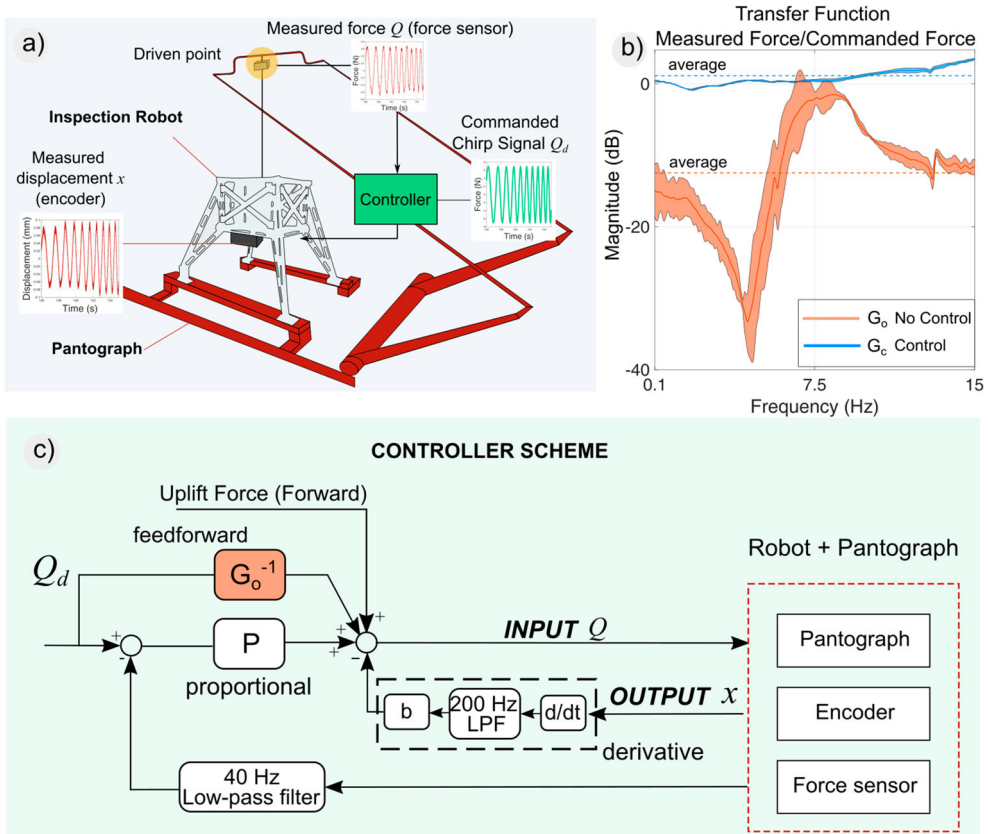
Figure 2. (a) Input-output architecture for pantograph dynamic test. (b) Magnitude plot (decibel scale) of the force transfer function (measured force against the reference signal) in the open-loop (no control) and in the closed-loop configuration. The confidence bands have been evaluated at $\pm 2\sigma$. (c) Schematic of the force control implemented to achieve homogeneous excitation throughout the frequency interval.

located at the middle span of the torsion bar. The output is the consequent structural displacement x which is measured through a digital encoder with resolution of $5 \cdot 10^{-2}$ mm.

The reference signal Q_d of the input force is generated by the controller and transmitted to the driven-point through a wire actuation. Tension in the steel wire (diameter 1.5 mm) is provided by a brushless DC motor with a direct drive connection. Positive tension in the wire is guaranteed throughout the dynamic test (level of the excitation ~ 10 N) because the wire transmission simultaneously applies a static force (~ 100 N) which is necessary to balance the uplift force of the pantograph. Nevertheless, due to disturbances, the real force Q applied to the pantograph differs from the desired force Q_d. Hence, the force sensor located directly at the driven-point, as in Figure 2(a), is essential for accurate characterisation of the dynamics because it allows measuring the true applied force. To this end, we adopted an analog force sensor, with an embedded bending parallelogram amplifier, providing a resolution of $5 \cdot 10^{-3}$ N.

The wire transmission was designed and validated for a bandwidth of 0–25 Hz. Hence we consider that the displacement of the actuator is equal to the vertical displacement of

the pantograph in the frequency interval of 0–15 Hz. Consequently, the structural response is measured through the digital encoder attached to the brushless motor. All signals are measured with 1000 Hz as the sampling rate. This value has been set upon considerations about the stability of the feedback loop that is used to control the true applied force Q. The operation of the robot is pursued through a host PC running a Matlab Simulink model in real-time. A 16-bit DAC board is used together with a communication module based on the EtherCAT protocol.

In this regard, when the nonlinear behaviour of the structure under test cannot be neglected, the control of the excitation source becomes a relevant issue. Indeed the input signal should be chosen to guarantee homogeneous energy across the whole frequency interval of the excitation. Nevertheless, the operation of any exciter involves undesired phenomena due to inertia and friction, whose effect is to introduce a difference between the commanded excitation signal Q_d and the truly applied excitation Q. In this sense, the use of the linear chirp as the commanded excitation signal reveals to be strategic. Indeed, notwithstanding the presence of distortions, dealing with a band-limited deterministic signal allows the possibility to conceive a control action to reject the effects of disturbances [31,32].

In Figure 2(c) it is shown the scheme of the force control. At each time step, the error between the reference dynamic force signal and the (low-pass filtered) measured force is estimated so that a control action is computed as the sum of a proportional-derivative term and a feedforward term, based on the experimental estimate of the force transfer function G_o, characterised during dedicated calibration tests, shown in Figure 2(b). The dynamic force is summed up to a further feedforward action corresponding to the static uplift force.

Figure 2(b) shows the estimates G_o of the force transfer function, in the form of a magnitude plot, in the so-called *open loop* configuration, that is without any control action, and in the *closed loop* configuration G_c in which feedback control is turned on when the level of the chirp excitation was set to 8 N (average level in the explored interval).

An ideal actuator, exempt from any disturbance, would produce a constant curve at 0 dB meaning an integral transmission of the desired force. Instead, the open-loop curve shows a pronounced drop-off around the first structural resonance at 3 Hz, where the transfer function reaches the minimum value of −40 dB. Except for a narrow band of about 5 Hz, where the curve almost reaches the value of 0 dB, the transfer function values stay always negative. The average value of −17 dB demonstrates how the force attenuation is persistently present in the spectrum. Instead, the control action achieves a sensibly improved spectral profile which is very close to the 0 dB, even though a slight increment in the frequency is still present. Nevertheless, the average value of the transfer function is found to be close to 0 dB. Besides, using force control reduces the variability of the applied excitation. Indeed the $\pm 2\sigma$ confidence band (15 repetitions) in the closed-loop configuration is more narrow, which is helpful in reducing the noise during the experimental estimation of the FRFs.

3.2. Parameters of operation

During the execution of structural dynamic tests the following parameters were introduced and controlled:

- Amplitude of the excitation: it is represented by the amplitude peak of the linear chirp signal during the frequency sweep. The following values were adopted: 2–8–14 N. Outside this range, some excitation is still possible but the measurements are affected by a sensibly higher noise with a decrease of the input-output coherence at the resonances which drops at about 0.5, meaning poor correlation. Additional values within this range were used in specific damage scenarios to assess the existence of a trend between the damage index and the excitation level;
- Average extension height: it represents the ideal average position of the pantograph during the test. This parameter mimics the height of the contact with the overhead line during the normal operation of the pantograph. Moreover, it influences the stiffness of the pantograph. Tests have been carried out for a single average position equal to 1700 mm;
- Tension of the wire: it represents the value of the static force applied on the pantograph to balance its uplift force. This parameter mimics the contact force during the normal operation of the pantograph and it influences the possible drift of the extension height which occurs at low-frequency and in the upward direction. The drifting of the position must be avoided because it affects the spectral estimate. The value of the tension has been tuned based on the experimental estimates of the pantograph lift and friction (see Section 3.3), and according to the amplitude of the excitation. Hence, when the amplitude of the excitation is equal to 2 and 8 N, the tension is 93 N, while when the amplitude of the excitation is 14 N, the tension is set at 95 N;
- Frequency of the excitation: it determines the number of vibration modes that can be excited during the dynamic test and it has a relevant impact on the effectiveness of the damage detection. In this experimental campaign, we adopted an interval of 0.1–15 Hz. The upper value is limited by the bandwidth of the device and the force-saturation limit of the closed-feedback loop. Above 15 Hz we observed a drop of the input-output coherence below 0.5 when the force level was set at the maximum value;
- Test duration: it influences the spectral resolution, i.e. the number of frequency bins that are included in the spectrum. In this experimental campaign, we adopted a duration of 150 s which ensures around 2250 points in the frequency interval of the excitation;
- Pressure of the pneumatic actuator: the pressure inside the pneumatic cylinder of the actuator reveals to slightly influence the stiffness of the lift force. For this reason, we kept constant the value of this parameter at 5.5 bar;
- Number of repetitions: a number of 10 repetitions was assumed for each of the investigated scenarios.

3.3. Static characterisation through speed-controlled tests

For the sake of completeness, we discuss the preliminary experiments of static characterisation of the pantograph, carried out through a so-called *controlled speed* test in which the inspection robot drives the pantograph along a series of repeated cycles of opening and closure. Feedback control is closed on the measured position of the pantograph to ensure that the speed is kept constant in each stroke. The acquisition system acquires position and force data.

In order to estimate the characteristic of the artificial damper test is repeated for increasing values of the speed. A reference value of 50 mm/s is defined by the European standard
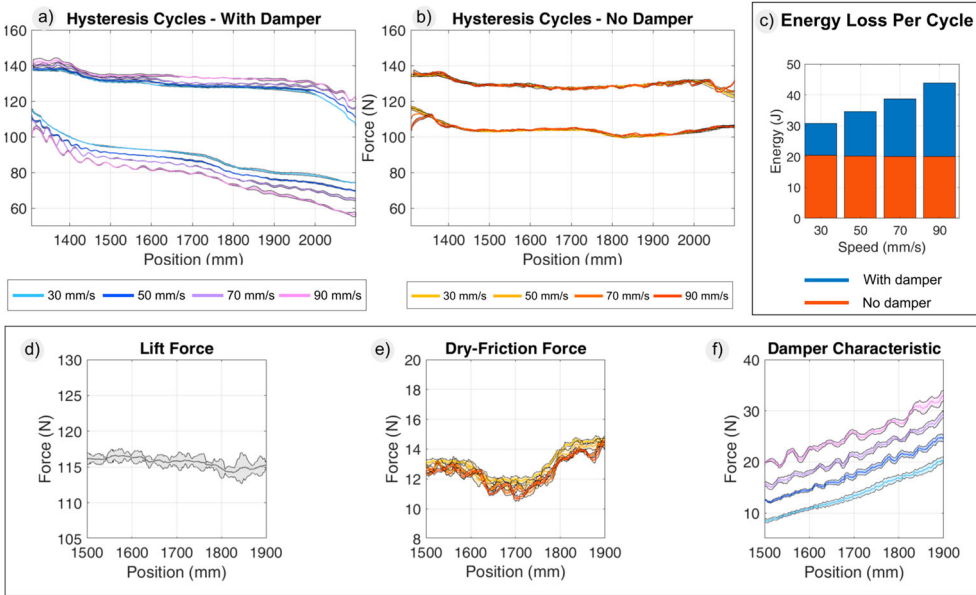
Figure 3. Static characterisation of a new pantograph through controlled speed tests. (a) Hysteresis cycles for increasing values of the speed in two configurations: (a) with the suspension damper; (b) without the suspension damper (b). (c) Energy loss per cycle with and without the damper. (d) Estimated uplift force. (e) Estimated dry-friction force at the different speed values. (f) Estimated damper characteristic (force against the position for different values of the speed).

[17] and it also coincides with the reference value adopted by commercial measurement devices (see also [7]). The lower limit of 20 mm/s has been found empirically as the threshold: under this value, the hysteresis force is found no more dependent on the speed. The upper limit is determined by the stability of the position controller and it corresponds to 90 mm/s. The amplitude of the stroke was set equal to 800 mm and its extremes are determined by physical limits: end-stroke of the pantograph (around 2200 mm from the ground) and vertical encumbrance of the inspection robot. All cycles have been repeated 10 times for each value of the speed and the pressure in the suspension has been kept constant to 5.5 bar.

The controlled speed test has been executed on a new pantograph (α in the following) in two configurations: with and without the damper. This is necessary to extricate from the hysteresis data the amount of friction damping that is due to the joints friction. The reference trajectory has been confronted with the real trajectory and a relative error below 1% has been found for all the values of the speed. In Figure 3(a,b) are shown the hysteresis cycles in the form of force-position diagrams with and without the damper respectively and for the four values of speed. It is found that the energy dissipated during the cycle, estimated by the area of the cycle, is proportional to the speed when the damper is present, Figure 3(c). Namely, the energy ranges from 30.8 to 43.9 J as the speed goes from 30 mm/s to 90 mm/s. Instead, the energy dissipated is almost constant when the damper is neglected with an average value of 20 J.

From diagram (a) it is possible to estimate the hysteresis force as the semi-amplitude of the cycle. It is found that the hysteresis force is dependent on the position of the pantograph

and the speed. Instead, without the damper, the hysteresis is independent of the speed and also of the position, as shown in Figure 3(e) since the dissipative force is only due to the dry-friction forces that are present on the joints. Indeed the forces are very close to an average value of 15 N that coincides with the normative prescription. Again, from diagram (b), it is possible to estimate the lift force generated by the main suspension of the pantograph.

From Figure 3(d), it is observed that by varying the position, the average lift stays constant around a value of 115 N. This value is dependent on the calibration procedure of the spring of the main suspension and it determines the stiffness of the contact force and the wear rate of the pan head and the high-voltage line. In diagram (d), we also indicate a confidence band at $\pm 3\sigma$ to show that the measured force has a few percentage variation from the mean value along the entire amplitude of the stroke. Indeed, according to the European standard [33], it must be ensured that the standard deviation of the contact force stays below 1/3 of the mean value.

The estimate of the characteristic curve of the damper can be pursued by the difference in the hysteresis cycles. The result is shown in Figure 3(f) where the force generated by the damper is plotted against the position of the pantograph for the four values of the speed test. It is observed that this damping term depends on both the position (it increases proportionally with the height of the pantograph) and the speed (in accordance with the viscous characteristic of these devices).

4. Methodology for damage diagnosis

4.1. Formulation of the hypothesis test

The diagnosis strategy, illustrated in Figure 4, consists of three phases: (i) vibration tests for multiple excitation levels, and estimation of the FRF; (ii) statistical analysis; (iii) synthesis of diagnosis based on the analysis of an aggregated damage index against the explored excitation levels.

In particular, the receptance FRF $H(\omega)$ (mm/N) is admitted as the characteristic feature, extracted from the measured spectra of the excitation Q and displacement X as follows:

$$H(\omega) = \frac{X(\omega)}{Q(\omega)} \tag{1}$$

The following hypothesis test is formulated comparing the FRF magnitude $|H^U(\omega)|$ of a pantograph under test in the unknown condition to that of the safe structure $|H^S(\omega)|$:

Null hypothesis (healthy structure) : $\delta|H(\omega)| = |H^S(\omega)| - |H^U(\omega)| = 0$

Alternative hypothesis (damaged structure) : $\delta|H(\omega)| = |H^S(\omega)| - |H^U(\omega)| \neq 0$ (2)

Since the true FRFs are unknown, we used the statistical estimates of the experimental frequency response functions $|\hat{H}|$, obtained as follows:

$$E|\hat{H}(\omega)| \approx |H(\omega)| \tag{3}$$

where the estimator is supposed to follow a Gaussian distribution. In Equation (1), we assumed a p-Welch estimate of the FRF, based on the input and output data record.
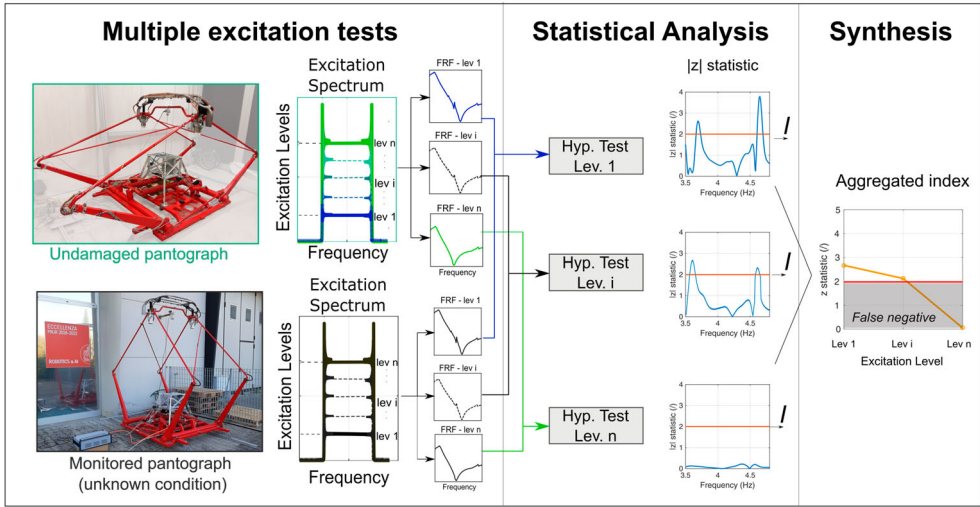
Figure 4. Schematic of the statistical method proposed for the diagnosis of the railway pantograph, based on the FRFs estimated at multiple levels of the input excitation.

Under the null hypothesis, the true FRF magnitudes collide ($|H^S(\omega)| = |H^U(\omega)|$). Hence $\delta|\hat{H}(\omega)| = |\hat{H}^S(\omega)| - |\hat{H}^U(\omega)| \sim \mathcal{N}(0, 2\sigma^2(\omega))$.

The variance $\sigma^2(\omega) = \text{var}|\hat{H}^S(\omega)|$ is also unknown but it may be estimated as follows:

$$\text{var}|\hat{H}^S(\omega)| \approx \frac{1 - \gamma^2(\omega)}{\gamma^2(\omega)\, 2K} \tag{4}$$

where γ^2 stands for the coherence function, and K stands for the number of segments used in the Welch spectral estimation.

At this point, the equality of the two FRF magnitudes is examined at a given α risk level through the statistical test:

$$z = \frac{|\delta|\hat{H}(\omega)||}{\sqrt{2\hat{\sigma}_S^2(\omega)}} \leq z_{1-\alpha/2} \tag{5}$$

where $z_{1-\alpha/2}$ stands for the standard normal distribution at the $1 - \alpha/2$ confidence level limit, i.e. at the 95% of confidence it turns out that $z_{1-\alpha/2} = 2$. In Equation (5), $\hat{\sigma}_S^2$ stands for the variance of the system in the safe condition.

If the condition expressed by Equation (5) is satisfied at all the frequency bins, then the null hypothesis is accepted and the pantograph under test is considered in the safe condition. Otherwise, there is evidence that damage has occurred. In this case, we define an aggregated damage index I, corresponding to the average value of the statistical test over the frequency interval:

$$I = \frac{\int_{\omega_i}^{\omega_f} z(\omega)}{\omega_f - \omega_i} \tag{6}$$

where: ω_i and ω_f represent the initial and final limits of the frequency interval, respectively.

Once the FRFs of some damage conditions have been acquired and labelled, it is possible an identification exercise. Indicative identification may be ascertained by confronting the results of the unknown structure with the labelled explored conditions:

$$\text{Hypothesis A (damage type A)} : |H^U(\omega)| \sim |H^A(\omega)|$$

$$\text{Hypothesis B (damage type B)} : |H^U(\omega)| \sim |H^B(\omega)| \qquad (7)$$

$$\cdots$$

where $|H^A|$, $|H^B|$ stand for the FRF estimated in the labelled scenarios A, B, as an example.

Due to nonlinearity, the hypothesis test is formulated for each value of Q_0 and the aggregated damage index is plotted against the excitation level. In the example of Figure 4, the aggregated index is above the threshold for level 1 and level i of the input excitation, while it falls in the region of false negatives, i.e. below the threshold, at the level n, suggesting the presence of a false negative when high values of the input excitation are employed. In such a case, when no clear accordance about the damage can be inferred from the values of the damage index over the excitation levels an ultimate decision is not taken, but further investigation is recommended,

4.2. Construction of the baseline

Characterisation of the pantograph in the undamaged state was pursued from a population of pantographs of the same type, classified as follows:

- *α-new pantograph*: data on this sample were acquired immediately after revision at the overhaul, i.e. this pantograph was repaired and subjected to a manual calibration procedure of the pneumatic actuation and it can be considered as new;
- *β-laboratory pantograph*: it is a pantograph revised at the overhaul in 2016 and sent to our laboratory only for experimental purposes, i.e. subjected to natural aging only under environmental conditions;
- *γ-overhaul pantograph*: it is a sample, revised in 2018, sent to the overhaul after visual inspection on the railway line, but which revealed to be a false positive due to the absence of clear damages and after verification of the uplift and damping forces;
- *δ-damage simulations pantograph*: it is a pantograph of the kind γ subject to simulated damages (Figure 5).

For each sample, the FRF is estimated at each level of the excitation with a confidence band at $\pm 2\sigma$ based on a number of ten repetitions of the dynamic test. Afterward, the baseline at a given excitation level is obtained by averaging data from the corresponding three pantographs. Figure 6 shows the magnitude plot of the FRFs on a decibel scale for each kind of pantograph and for each excitation level.

It emerges a significant variability in the FRFs, especially in the range of 10–15 Hz, despite all of them being considered in an undamaged state. The main difference between these pantographs is concerned with aging and evident wear which in turn is reflected by an increasing level of dry-friction at the joints from the pantograph α to the pantograph γ. In this regard, it is known, [34], that different ratios of the dry-friction over the excitation amplitude (friction ratio) have a sensitive role in the profile shape of the FRF. Based on
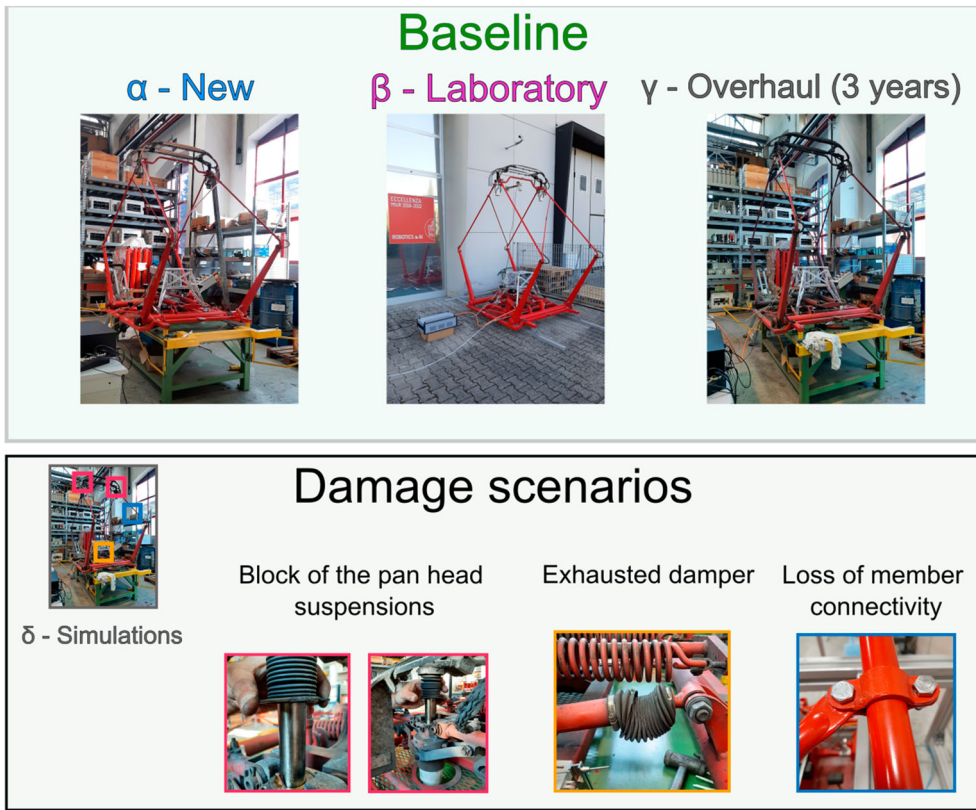
Figure 5. Characterisation of pantograph in the undamaged condition through the acquisition of measurements from a population of pantographs of the same kind but with different aging. Below: simulated damage scenarios.

the friction ratio, the response of the pantograph at the driven-point can be of three kinds: continuous, stick-slip, or stuck. The onset of these regimes depends on the equilibrium of each rotational pair and it also changes with the frequency.

During a vibration test, multiple stick modes may arise in which different subsets of the joints stay stuck. Thus, the response of the pantograph may result complex in an identification sense because the modal parameters are found dependent on the excitation level. For example, from Figure 6, it is observed that with increasing the excitation level, the first resonant peak is decreased in magnitude and damping. Besides, also the frequency of the peak is shifted towards the lower frequencies. As an example, for the pantograph α, the first peak, located at around 3 Hz for the low excitation level, results completely dampen out at 14 N where no resonant behaviour emerges.

4.3. Damage scenarios

In this experimental study, three damage scenarios have been considered. The first is concerned with the block of the pan head suspension. Such a scenario can occur during normal operation of the pantograph due to oxidation of the springs that are devoted to supporting
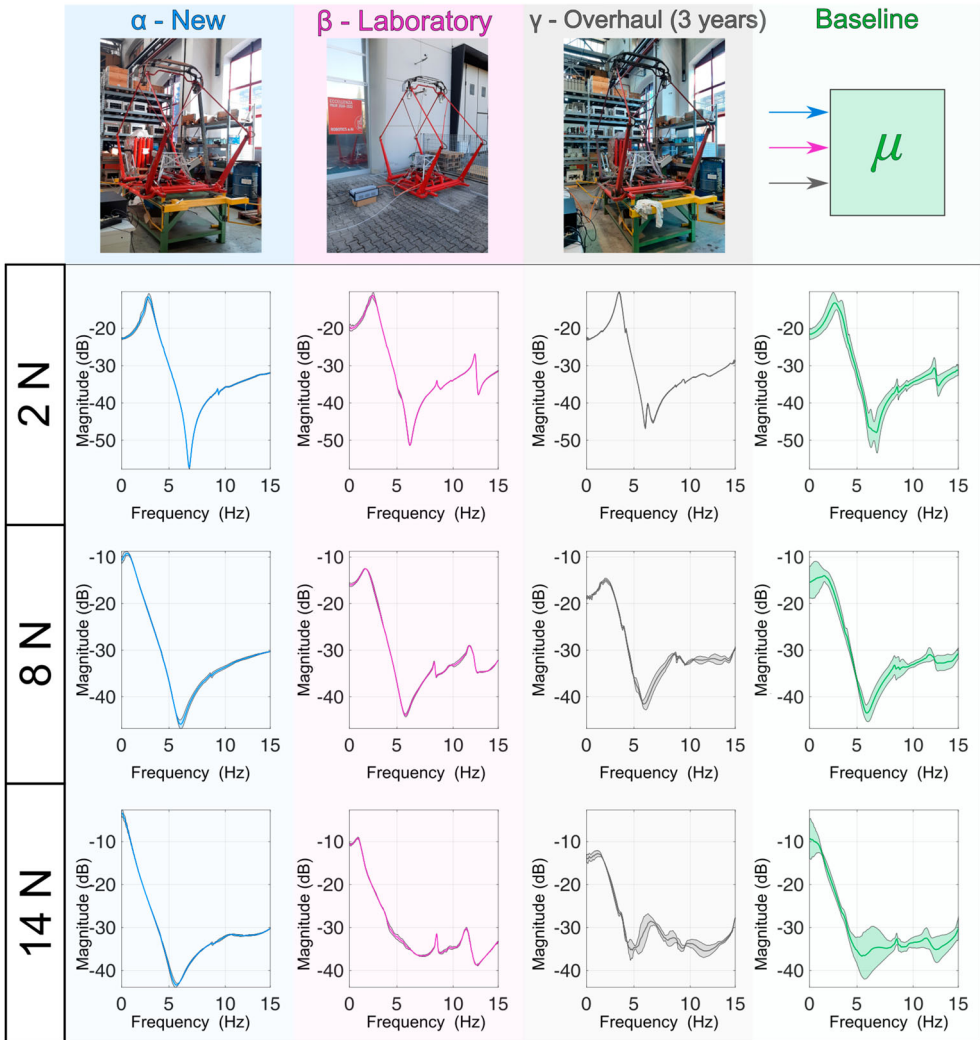
Figure 6. Baseline construction extracted from the three pantograph samples which were considered in an undamaged condition. The baseline at $\pm 2\sigma$ was obtained by averaging the magnitude Frequency Response Function (decibel scale) referred to each pantograph. The estimate in the interval 0.1–15 Hz was repeated on three values of the excitation amplitude.

the pan head. After the block of the suspension has occurred, the pan head is constrained to the pantograph mechanism, and no relative motion is allowed in the vertical direction. This phenomenon is particularly crucial for the safety and operation of the pantograph because the normal dynamic operation of the pan head suspension determines the quality of the contact force and the wear of the pantograph mechanism. For this kind of damage, we explored three conditions, namely the block of the right suspension, the block of the left suspension, and then the simultaneous block of both suspensions.

The second damage scenario is concerned with the hydraulic damper of the pantograph actuation. Common faults in the damper are the break of the sealings or the sticking of the

piston which in turn imply a large variation of the viscous damping capability. In this work, we focussed on the leakage of the oil – exhaustion of the damper.

The last damage scenario is concerned with the loss of member connectivity in the bolted connections. During normal operational life, bolted joints are prone to the reduction of preload which might induce a loss of joint stiffness. In this research, we chose the bolted connection between one diagonal bar and one of the upper arms of the pantograph. Such a damage scenario represents a local and subtle alteration to the structural integrity of the pantograph. Indeed, the main purpose of the diagonal bar is to provide lateral stiffness, through the connection of the two parallelograms of the pantograph mechanism. Nevertheless, due to the structural redundancy, this purpose is still accomplished in the damaged scenario, even if the stiffness of the pantograph is reduced.

5. Results

In the following, we discuss the analysis of the structural dynamic tests carried out for the three kinds of damages discussed in Section 4.3. In Figures 7–9, the baseline is represented by a green line and a confidence band at $\pm 2\sigma$.

5.1. Damage detection and identification

Figure 7 shows the FRFs for the three damage scenarios that are concerned with the block of the pan head suspension (right in dark grey, left in grey, and combined, i.e. right + left in magenta). Some qualitative damage features that occur independently of the scenario and the level of the excitation are:

- the dominant resonance peak is increased in magnitude;
- the drop around the zero is enhanced by the damage;
- the structural resonance peaks appear with a sharpened shape.

In particular, at 2 N, the maximum error achieves a value of 9.74 dB at 11.96 Hz. At 8 N, the maximum error falls at the zero, at 6.14 Hz, with a magnitude of 8.98 dB. In the same fashion, at 14 N, the maximum error is observed at the zero, at 5.97 Hz, with a magnitude of 13.63 dB.

Figure 8 shows the FRFs for the damage scenario concerned with the exhausted damper (yellow line). A softening behaviour can be observed in the frequency range of 0.1–3 Hz since the dominant resonance peak is shifted towards a lower frequency. Moreover, for the excitation levels of 8 N and 14 N, the magnitude of the peak is increased by 11 dB and 18 dB, respectively and representing the maximum error. No significant error is produced around the peaks that are concerned with the structural modes of the pantograph. This is due to the non-collocation of the damper which is effective only on the opening and closure mode of the pantograph while it is non-collocated with the displacement of the driven-point for any of the structural modes.

Figure 9 shows the FRFs concerned with the loss of member connectivity (blue line). Being a subtle damage, the error produced on the FRF is less evident compared with the other scenarios. Moreover, the error is concentrated only on two frequency intervals: 3.5–3.7 Hz, and 4.5–4.7 Hz.
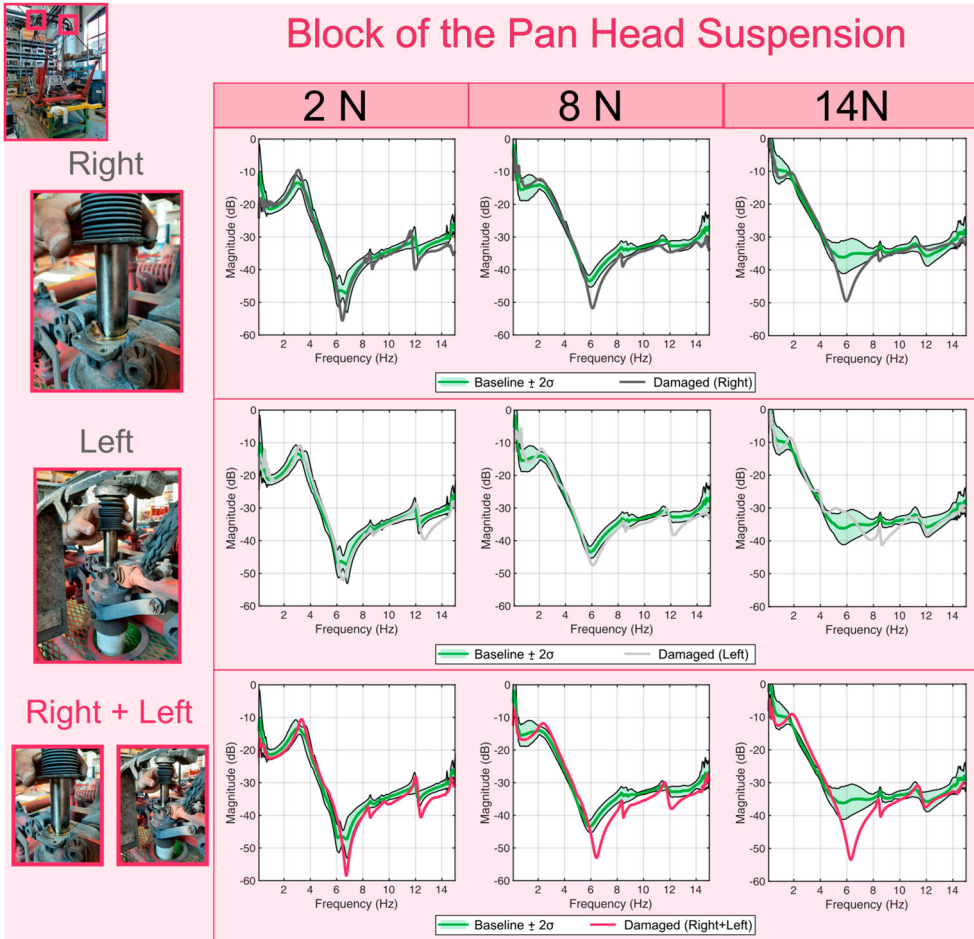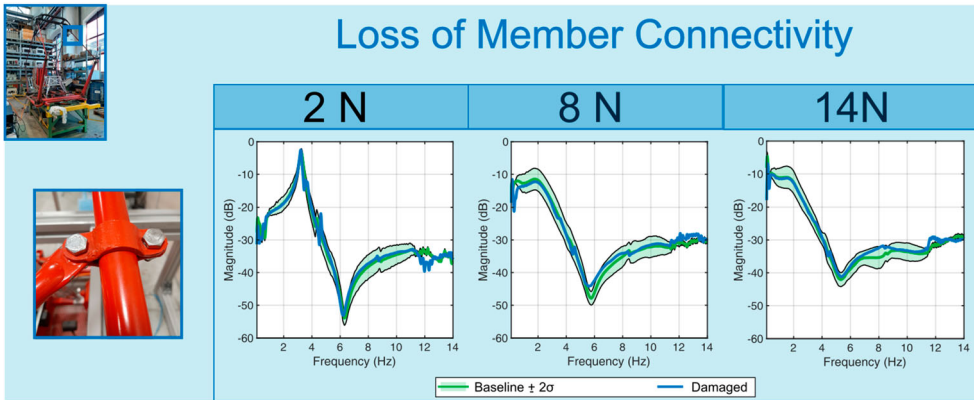
Figure 7. Comparison of the Frequency Response Functions in the case of a block of the pan head suspension (right, left, and combined: right + left simultaneously) with the baseline for three distinct levels of the input excitation.
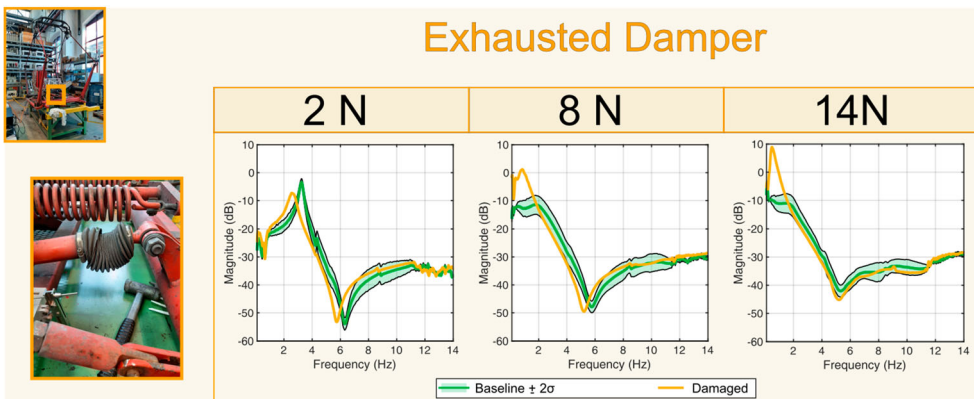
Figure 8. Comparison of the Frequency Response Functions in the case of the exhausted damper with the baseline for three distinct levels of the input excitation.

Figure 9. Comparison of the Frequency Response Functions in the case of loss of member connectivity at a bolted joint with the baseline for three distinct levels of the input excitation.

Indeed, the loss of connectivity between the diagonal bar and the upper arm of the pantograph introduces two additional structural modes coinciding with the bending modes of the bar. These modes are reflected in the response of the driven-point and two spiky resonance peaks can be observed at the low level of the excitation. The interesting point is that increasing the level of the excitation implies progressive damping of these damage-induced peaks, which tend to disappear at high levels of excitation. Such evidence is related to the transition of the system from the stick regime, for a low excitation level, to the continuous motion regime at a high excitation level. Based on the dynamic properties of the pantograph, the resonant peak of the bar in the damaged condition is emphasised when the vibration occurs in a stuck regime.

Figure 10 shows the indicative identification of a damage scenario. As an example, a new set of data was collected in the case of a pantograph with an exhausted damper. This set was generated by simulating the exhaustion of the damper on the pantograph β. Therefore, the new and labelled damaged FRFs have been confronted with the previous damage scenarios (pan head suspension and loss of member connectivity) and with the previous set of data on the exhausted damper. The same colour legend of Figures 7–9 has been applied. In this case, the baselines at $\pm 2\sigma$ represent the damaged scenarios. The same procedure was performed for the other damage types.

Instead, Figure 11 is devoted to a validation test in which a set of new FRF is estimated from the undamaged pantograph – type β – and it is confronted with the baseline. Slight differences emerge around the first peak, the zero, and the structural resonances. This is due to the normal variance of the system, related to errors in the parameters discussed in Section 3.2, in particular, the value of the tension, the average position of the pantograph, and misalignments.
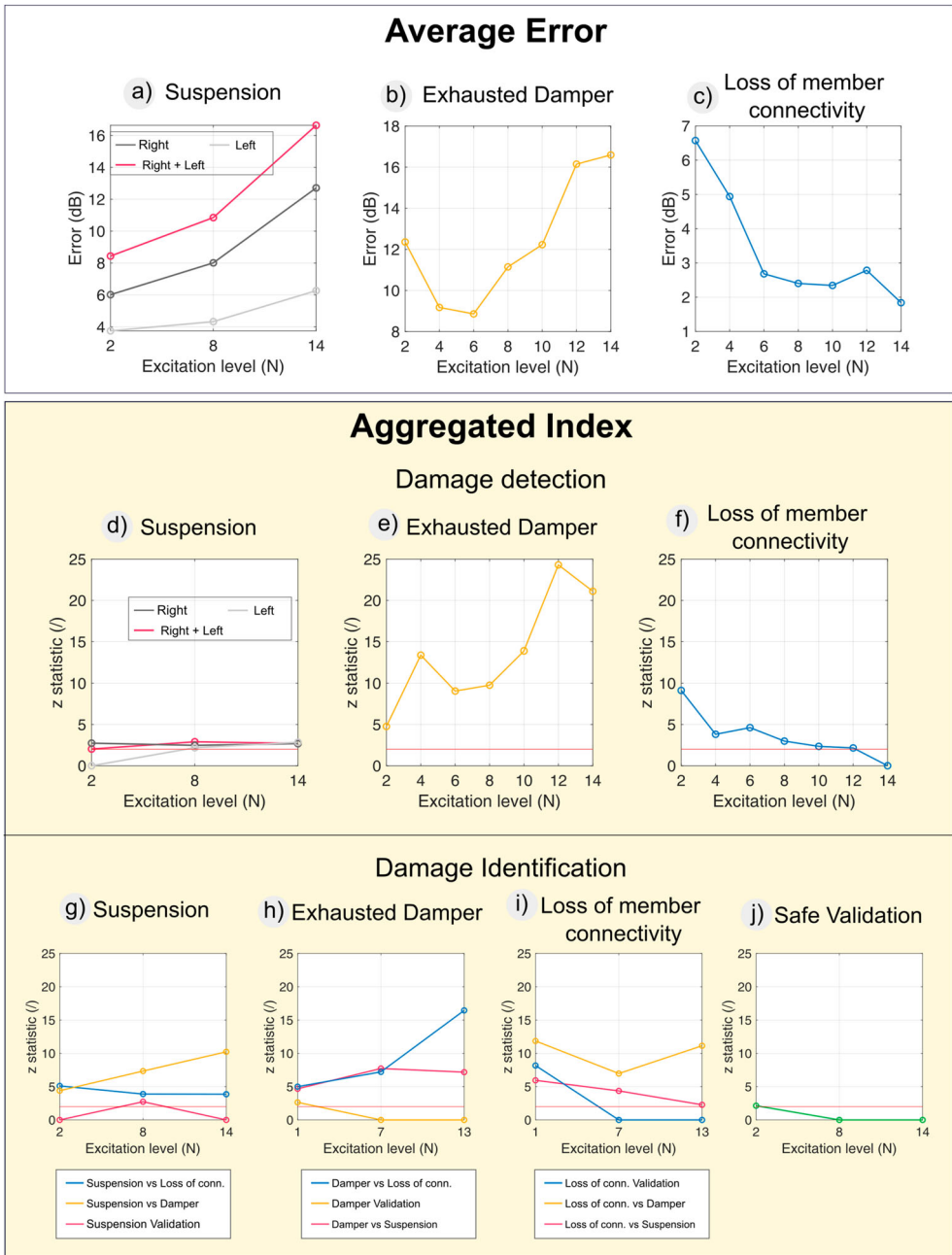
5.2. Aggregated index

Indicative damage detection results are represented in Figure 12, where we plot the average error and the aggregated index against the threshold at the 95% of confidence.
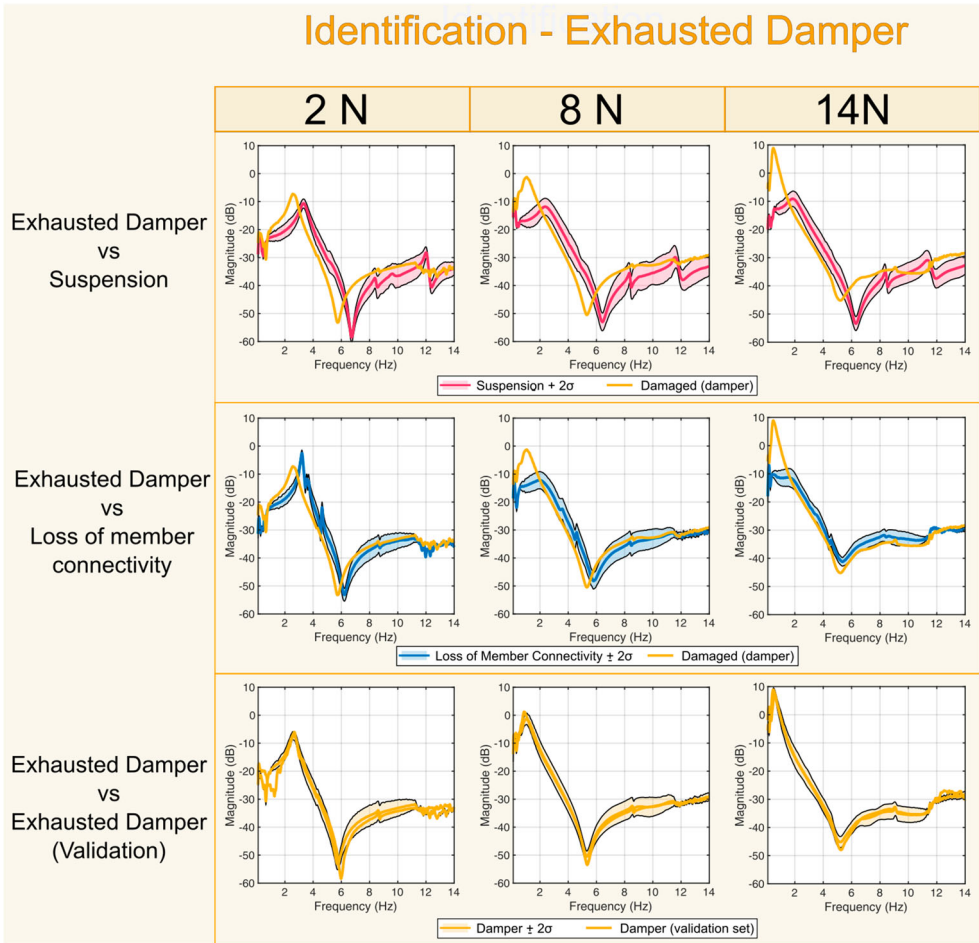
Figure 10. Example of indicative damage identification: a new set of Frequency Response Functions is acquired in the case of exhausted damper and confronted with the Frequency Response Functions of the other labelled damage types.
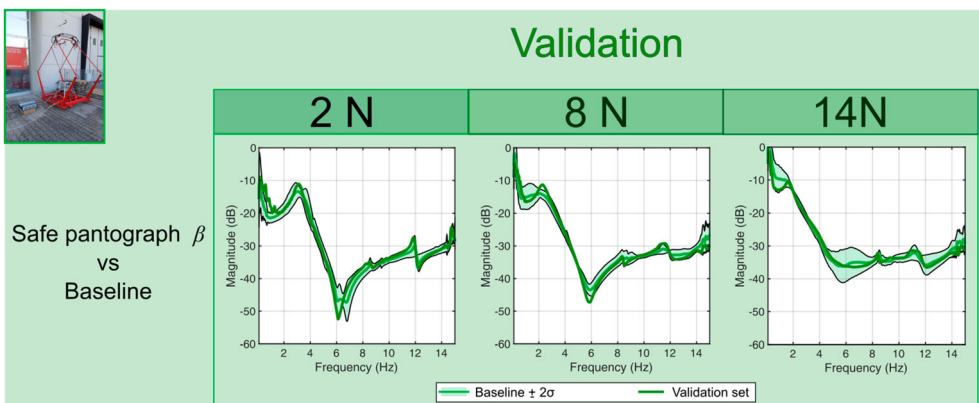
Figure 11. Example of indicative validation of the baseline: a new set of Frequency Response Functions is acquired from a pantograph in the undamaged condition and confronted with the baseline.

Figure 12. Analysis of the aggregated damage index against the level of the excitation. (a)–(c) Average error (damage vs baseline). (d)–(f) Statistical error and (g)–(j) Identification.

In Figure 12(a–c) the average error is shown on a decibel scale. In Figure 12(a) we observe that the block of the pan head suspension is influenced by the excitation level since the average error increases with the excitation level for all three explored scenarios. Namely, the average error almost doubles when the excitation is increased from the low

to the high level. Nevertheless, the average error shows different values between the block of the right and the left suspension. Instead, blocking both suspensions produces higher values of error for each level of the excitation.

The exhausted damper produces the highest values of error among all the explored damage scenarios, despite the discrepancies being concentrated only on the 0.1–3 Hz interval of the spectrum. As it will be shown later, this case is particularly interesting also in a statistical sense. Consequently, we decided to repeat the experiments for further levels of the excitation, ranging in the interval $2:2:14$ N, for a total number of seven levels of the excitation. Despite some oscillation, a clear trend of increasing error with the excitation amplitude is found.

The same fitting procedure on the excitation level was performed in the case of loss of member connectivity, in Figure 12(c). Contrariwise, as the excitation level is increased, the error decreases, due to the damping effect on the damage-induced resonances which was observed in Figure 9.

Figure 12(d–f) reports the aggregated index on a fixed scale (0–25) for all the investigated scenarios. The threshold at the 95% of confidence is also plotted with a red horizontal line (corresponding to $z = 2$). In Figure 12(d) we observe that the statistical error concerned with the block of the pan head suspension is not dependent on the excitation level since the block of the right suspension is detected for all three levels of the excitation with values around 2.6. Contrariwise, the block of the left suspension is not detected (false negative) at the low level of the excitation, while similar values as in the right suspension case are found at 8 N and 14 N. Close values of the statistic are found for the block of both suspensions.

In Figure 12(e) we observe that the exhausted damper is always detected since the value of the statistic is sensibly above the confidence threshold for all the seven values of the excitation level. Besides, the trend that was shown for the average error is confirmed, since the statistical error increases with the excitation level by a factor of around 4.

In Figure 12(f), it is confirmed that the error concerned with the loss of member connectivity decreases with the excitation level. In particular, for the highest value of the excitation of 14 N, the damage is not detected (false negative).

The values of the aggregated index and the number of false negatives are reported in Table 1.

Results from the identification routine are shown in Figure 12(g–j). The test statistic always exceeds the threshold when testing the hypothesis between different damage types. Hence we can exclude confusion between different damage scenarios. On the other side,

Table 1. Aggregated index values and observed false negatives during the damage detection exercise.

Damage detection				
	Aggregated Index			
	2 N	8 N	14 N	False negatives
Suspension right	2.74	2.47	2.68	0
Suspension left	**0**	2.19	2.84	1
Suspension both	2.03	2.90	2.70	0
Exhausted Damper	4.76	9.76	21.11	**0**
Loss of member connectivity	9.13	2.99	0	1

Table 2. Fail cases observed in the indicative identification exercise.

	Damage identification			
	Fail number	Fail case	Fail exc. level	Agg. index value
Suspension both	1	Suspension both	8 N	2.73
Exhausted damper	1	Exhausted damper	2 N	2.64
Loss of member connectivity	1	Loss of member connectivity	2 N	8.17

for all three damage scenarios, a false positive has been found in the validation test - that is when confronting different sets of the same damage scenario, as listed in Table 2 where we report the fail, i.e. not identified scenarios. This occurs at the middle excitation level for the block of the suspension, where the statistic achieves a value of 2.73, and at the low excitation level for the case of exhausted damper and loss of member connectivity. In the case of the exhausted damper, the error is close to the threshold being equal to 2.64. The same behaviour is observed in the validation of the safe condition, Figure 12(j), since no false positives are found, except for the low value of the excitation where the statistic achieves a value of 2.14, just above the threshold.

6. Conclusions

In this work, we addressed the problem of damage assessment in the railway pantograph mechanism. With respect to previous literature, we discuss an in-depth investigation of the pantograph nonlinear behaviour and uncertainties for three damage conditions affecting the pan head suspension, the damper of the actuation, and the connectivity of a bolted connection. To this purpose, the experimental assessment was pursued through a dedicated inspection robot that we designed and validated for periodic and fast inspection of the pantograph integrity in the frequency interval 0–15 Hz.

The proposed results rely on accurate control of several parameters that we discussed and, in particular, of the input excitation whose amplitude is controlled at all frequencies through a control strategy that was implemented by the dedicated robotic actuation. Hence a hypothesis test was formulated for the frequency response function of the pantograph in the safe and damaged condition which were estimated for different levels of the input excitation. In this way, it was ascertained whether fine control of the excitation level can be exploited to damage diagnosis. At the same time, the typical gross variability between pantograph samples was also considered by acquiring data from a family of four pantograph samples with different operational lives, and aging conditions.

Results suggest that information deriving from different excitation levels can be useful in the damage detection phase. Indeed, detecting damage at more excitation levels provides further significance that damage has occurred. As an example. in the case of the block of the pan head suspension, the damage was not recognised at the low level of the excitation, but it is detected on the other two. Consequently, such evidence could suggest further investigations. Besides, the exploration of the excitation force revealed more useful for the case of loss of member connectivity and in the case of an exhausted damper, where the damage index is found to follow a clear trend with the excitation level (of decrease and increase respectively). Moreover, indicative damage identification was achieved showing the potentiality of the proposed device and methodology for pantographs diagnosis. Still, some false

positives were found at the low levels of the input excitation where the pantograph response is more sensitive to boundary conditions due to higher frictional nonlinearity.

In the future, we aim to develop a mature version of our prototype that allows further sensor channels and faster setup with the aim to test a broader population of pantographs subject to a multitude of damage conditions.

Acknowledgments

Disclosure statement

References

[1] RAIB. Report 06/2013: accident involving a pantograph and the overhead line near Littleport. 2013.
[2] Conway S. Review of human factors risk in rail vehicle maintenance and inspection. 2008.
[3] Conway S. Lump mass models for legacy pantographs on GB mainline. 2016. (T1105 Report).
[4] Peters J. Dead line testing of pantographs on the RTT catenary system. 1981.
[5] Park TJ, Han CS, Jang JH. Dynamic sensitivity analysis for the pantograph of a high-speed rail vehicle. J Sound Vib. 2003;266(2):235–260. doi: 10.1016/S0022-460X(02)01280-4
[6] Pombo J, Ambrósio J. Influence of pantograph suspension characteristics on the contact quality with the catenary for high speed trains. Comput Struct. 2012;110:32–42. doi: 10.1016/j.compstruc.2012.06.005
[7] Xin T, Roberts C, Weston P, et al. Condition monitoring of railway pantographs to achieve fault detection and fault diagnosis. Proc Inst Mech Eng F. 2018. doi: 10.1177/0954409718800567.
[8] Seering W, Armbruster K, Vesely C, et al. Experimental and analytical study of pantograph dynamics. J Dyn Syst Meas Control. 1991;113(2):242–247. doi: 10.1115/1.2896371
[9] Collina A, Bruni S. Numerical simulation of pantograph-overhead equipment interaction. Veh Syst Dyn. 2002;38(4):261–291. doi: 10.1076/vesd.38.4.261.8286
[10] Ambrósio J, Pombo J, Rauter F. A memory based communication in the co-simulation of multi-body and finite element codes for pantograph-catenary interaction simulation. In: Multibody Dynamics. 2009. p. 231–252. (Compuational methods and applications). Springer, Berlin.
[11] Deml J, Baldauf W, Bahn AD. A new test bench for examinations of the pantograph-catenary interaction. In: Proceedings of the WCRR, Cologne, Germany; 2001. p. 25–29.
[12] Collina A, Facchinetti A, Fossati F, et al. Hardware in the loop test-rig for identification and control application on high speed pantographs. Shock Vib. 2004;11(3–4):445–456. doi: 10.1155/2004/740146
[13] Bruni S, Ambrosio J, Carnicero A, et al. The results of the pantograph–catenary interaction benchmark. Veh Syst Dyn. 2015;53(3):412–435. doi: 10.1080/00423114.2014.953183
[14] Collina A, Bruni S, Facchinetti A, et al. Pcada statement of methods. Veh Syst Dyn. 2015;53(3):347–356. doi: 10.1080/00423114.2014.959027
[15] Ambrósio J, Pombo J, Antunes P, et al. Pantocat statement of method. Veh Syst Dyn. 2015;53(3):314–328. doi: 10.1080/00423114.2014.969283
[16] Massat JP, Balmes E, Bianchi JP, et al. Oscar statement of methods. Veh Syst Dyn. 2015;53(3):370–379. doi: 10.1080/00423114.2015.1005016
[17] CENELEC. Railway applications – current collection systems – validation of simulation of the dynamic interaction between pantograph and overhead contact line. 2018.
[18] Xie C, Long Z, Peng X, et al. System's device of locomotive pantograph characteristic inspection. Patent ref.: CN204788991 (U). 2018. Available from: https://bit.ly/2GPrOUp.

[19] Bing C, Xu S, Gao Y, et al. Pantograph test method, system, device and rail vehicle. Patent ref.: CN106338405 (A). 2018. Available from: https://bit.ly/2UN8k6K.

[20] Lu G. Portable pantograph tester. Patent ref.: CN2316662 (Y). 1998. Available from: https://bit.ly/2IZLTcd.

[21] Yang H, Huang S, Gao Y, et al. Portable rail vehicle pantograph static test [of pressure] device. Patent ref.: CN205027525 (U). 2010. Available from: https://bit.ly/2LbCD7v.

[22] Li S, Li S. Static characteristic precise detection adjusting system for subway pantographs. Patent ref.: CN204462777 (U). 2015. Available from: https://bit.ly/2vroeJK.

[23] Xuzhing C, Dijun L, Wei H, et al. Pantograph test bench. Patent ref.: CN201803855 (U). 2011. Available from: https://bit.ly/2XXDqdX.

[24] Watanuki N, Kobayashi T, Shiono K, et al. Pantograph pushing-up force inspection device. Patent ref.: JP2017167068 (A). 2017. Available from: https://bit.ly/2GQGtPf.

[25] Zhang C, Liu L. Train pantograph structural health monitoring system. Patent ref.: US2018208222 (A1). 2018. Available from: https://bit.ly/2LjFew2.

[26] Villani LG, Shiki SB, Cunha A, Jr., et al..Challenges for structural health monitoring: non-linearities and uncertainties. In: Uncertainty Modeling: Fundamental Concepts and Models, III, University of Brasilia (UnB), 2022. p. 258–278, Book series in Discrete Models, Inverse Methods, & Uncertainty Modeling in Structural. 2022 hal-03811571.

[27] Vamvoudakis-Stefanou KJ, Sakellariou JS, Fassois SD. Vibration-based damage detection for a population of nominally identical structures: unsupervised multiple model (mm) statistical time series type methods. Mech Syst Signal Process. 2018;111:149–171. doi: 10.1016/j.ymssp.2018.03.054

[28] Santamato G, Chiaradia D, Solazzi M, et al. A robotic device for the structural dynamics inspection of railway pantographs through nonlinearity tests. IFAC-PapersOnLine. 2020;53(2):8476–8481. doi: 10.1016/j.ifacol.2020.12.1429

[29] Kopsaftopoulos FP, Fassois SD. Vibration based health monitoring for a lightweight truss structure: experimental assessment of several statistical time series methods. Mech Syst Signal Process. 2010;24(7):1977–1997. doi: 10.1016/j.ymssp.2010.05.013

[30] Santamato G, Chiaradia D, Solazzi M, et al. A lightweight robotic device based on a micro-macro actuation concept for the inspection of railway pantograph. J Mech Robot. 2020;12(6):Article ID 061002. doi: 10.1115/1.4046995

[31] Mayes RL, Gomez AJ. Part 4: what's shakin', dude? Effective use of modal shakers. Exp Tech. 2006;30(4):51–61. doi: 10.1111/ext.2006.30.issue-4

[32] Worden K, Farrar CR, Haywood J, et al. A review of nonlinear dynamics applications to structural health monitoring. Struct Control Health Monit. 2008;15(4):540–567. doi: 10.1002/stc.215

[33] CENELEC. Railway applications – current collection systems – requirements for and validation of measurements of the dynamic interaction between pantograph and overhead contact line. 2012.

[34] Lampaert V, Swevers J, Al-Bender F. Impact of nonlinear friction on frequency response function measurements. In: Proceedings of the International Seminar on Modal Analysis; Vol. 1. Citeseer; 2001. p. 443–450.